Weakly ($x=0$) and randomly ($x=0.033$) coupled Ising antiferromagnetic planes in $(Li_{1-3x}Fe_x)NiPO_4$ compounds

D. Vaknin, J. L. Zarestky, and J. E. Ostenson
Ames Laboratory and Department of Physics and Astronomy, Iowa State University, Ames, Iowa 50011

B. C. Chakoumakos
Oak Ridge National Laboratory, Oak Ridge, Tennessee 37831

A. Goñi
Departmento Química Inorgánica (ISEM), Facultad de Ciencias, Universidad del País Vasco/Euskal Herriko Unibertsitatea, A.P. 644, 48080 Bilbao, Spain

P. J. Pagliuso
Instituto de Física, UNICAMP, 13087-970 Campinas, São Paulo, Brazil

T. Rojo
Departmento Química Inorgánica (ISEM), Facultad de Ciencias, Universidad del País Vasco/Euskal Herriko Unibertsitatea, A.P. 644, 48080 Bilbao, Spain

G. E. Barberis
Departmento Química Inorgánica (ISEM), Facultad de Ciencias, Universidad del País Vasco/Euskal Herriko Unibertsitatea, A.P. 644, 48080 Bilbao, Spain
and Instituto de Física, UNICAMP, 13087-970 Campinas, São Paulo, Brazil

(Received 16 October 1998; revised manuscript received 22 February 1999)

Neutron diffraction and magnetic susceptibility studies of $(Li_{1-3x}Fe_x)NiPO_4$ ($x=0$ and $x=0.033$) compounds reveal remarkable differences between the magnetic properties of pure $LiNiPO_4$ and those of its lightly iron-doped derivative. The spin system associated with the Ni^{2+} ions ($S=1$) in the pure compound undergoes a collinear antiferromagnetic ordering at $T_N=19.1\pm0.5$ K, with the characteristics of weakly coupled two-dimensional (2D) Ising square planes. By contrast, randomly intercalated iron spins (in Li sites) between Ni^{2+} planes comprise a spin-glass-like subsystem which, despite their minute amount, drives the antiferromagnetic transition to higher temperatures $T_N=25.2\pm0.5$ K, and significantly modifies the critical behavior of the 2D Ni^{2+} system. It is argued that the doped compound can serve as a model system for studying the randomly coupled planar Ising model. [S0163-1829(99)15425-0]

I. INTRODUCTION

The physical and chemical properties of metal oxides such as phosphates and silicates are of interest because of their potential applications in the areas of ion exchange, intercalation, sorption, catalysis, and others.[1] These materials exhibit a variety of structural features, the most prominent of which is the existence of tunnels in which small ions can move freely; a property that makes them potential hosts for the insertion and extraction of ions as cathode materials in rechargeable batteries.[1–3] In addition, depending on the choice of metal ions, well-defined low-dimensional systems in the form of chains or layers of magnetic ions can be identified in these compounds, making these materials suitable candidates for exploring low-dimensional physical systems.[4]

$LiNiPO_4$ belongs to the olivine family of lithium orthophosphates $LiMPO_4$ (M=Mn, Fe, Co, and Ni) (Ref. 3) with space group *Pnma*. It has an elongated *a* axis, of length that is about twice the *b* and *c* cell constants,[3] with a structure that is comprised of nearly close-packed oxygen atoms in hexagons, with Li and Ni ions that are located at the center of octahedral sites and P ions that are in tetrahedral sites. The NiO_6 octahedra are corner shared and cross-linked with the PO_4 tetrahedra, forming a three-dimensional network, with tunnels along the [010] and [001] directions occupied by Li ions. However, the structure is closely packed compared with other Li-metal phosphates,[3] allowing for little ionic hopping. In principle, Li mobility can be increased by introducing vacancies in the Li sites, by exchanging several Li ions by a single di- or trivalent transition metal ion, preserving the charge balance in the system. Such substitutions by Fe^{3+} for three Li^+ ions yielded $(Li_{1-3x}Fe_x)NiPO_4$ for $x=0$, 0.03, 0.06, and 0.1 as identified by both ^{7}Li and ^{31}P NMR spectra and Mössbauer measurements.[5–7] Our neutron scattering studies are aimed at shedding light on the feasibility of such an approach to increase the Li mobility.

All members of the $LiMPO_4$ family (M=Mn, Fe, Co, Ni) contain buckled MO layers that are stacked along the *a* axis. There is a relatively strong antiferromagnetic (AF) coupling between nearest-neighbor (NN) transition-metal ions in the plane by superexchange interaction through an oxygen bond M-O-M.[8–10] However, there is no direct or superexchange

coupling between the moments in different planes, and only higher-order exchange interactions involving the phosphate group are possible (M-O-P-O-M as suggested by Mays[11]). This strongly suggests that these systems exhibit quasi-two-dimensional (quasi-2D) magnetic behavior.

Here we report on structural and magnetic neutron scattering and magnetic susceptibility studies of $(Li_{1-3x}Fe_x)NiPO_4$ ($x=0$ and 0.033). Santoro *et al.*[8,10] reported on the magnetic structure and susceptibility of the $LiMPO_4$ group (M=Fe, Co, Mn, Ni); however, due to the weak magnetic intensities from $LiNiPO_4$ the magnetic structure was not fully determined.[8] In reexamining the pure $LiNiPO_4$ compound we wish to elaborate on previous studies in two respects by determining the magnetic structure of $LiNiPO_4$, including the magnitude and direction of the magnetic moments,[12] and by characterizing the 2D nature of the magnetic system as discussed above. Then, by comparing the pure system to the iron-doped one, the effect of minute magnetic impurities inserted between the NiO planes can be better understood. In the past, randomly distributed atomic substitutions in pure compounds yielded intriguing as well as useful systems such as doped semiconductors, spin glass materials, and superconductors. Such substitutions can have profound effects on electronic band structures and on critical phenomena. As demonstrated below, a minute amount of Fe substitution in $LiNiPO_4$ dramatically modifies the magnetic properties of the pure compound.

II. EXPERIMENT

Neutron scattering measurements were carried out on the HB-1A triple-axis spectrometer at the High Flux Isotope Reactor (HFIR) at Oak Ridge National Laboratory. A monochromatic neutron beam of wavelength $\lambda=2.368$ Å ($k_0=2\pi/\lambda=2.653$ Å^{-1}) was selected by a double monochromator system using the (002) Bragg reflection of highly oriented pyrolytic graphite (HOPG) crystals. The $\lambda/2$ component in the beam was removed (to better than 1.3 parts in 10^4) by a set of HOPG crystals situated between the two monochromating crystals. The polycrystalline samples (of volume ≈ 8 cm^3) were sealed in thin-walled vanadium cans under He environment and mounted in a Heliplex (APD Cryogenics Inc.) closed-cycle He refrigerator for measurements. The collimating configuration used was 40′,40′,S,34′,68′. Magnetic susceptibility measurements were performed on a superconducting quantum interference device (SQUID) magnetometer (Quantum Design MPMS) on the same samples that were used for the neutron scattering experiments.

$LiNiPO_4$ was prepared by solid state reactions of LiOH, $Ni(NO_3)_2\cdot 6H_2O$, and $H_2NH_4PO_4$. For the doped phases, $Fe(NO_3)_3\cdot 9H_2O$ was included as a starting component. The starting materials were ground together in an agate mortar, and the resulting mixtures were heated at 573 K for 1 h and subsequently at 923 K for another hour to decompose the phosphates and nitrates. The resulting mixture was then kept for 20 h at 1023 K with an intermediate regrinding after 10 h. The final products were then quenched from 1023 K to room temperature.[13,14] The contents of Li, Fe, Ni, and P in the products was determined by ICP-AES analysis confirming the chemical formula $(Li_{1-3x}Fe_x)NiPO_4$. The compounds were characterized by x-ray powder diffraction method, using Cu $K\alpha$ radiation, confirming a single phase. Mössbauer experiments indicated that all of the the iron ions are of Fe^{3+} type in a single phase, with a minute secondary phase (less than 2%), corresponding to the $Li_3Fe_2(PO_4)_3$ phase, which was not observed in the x-ray diffraction.[15]

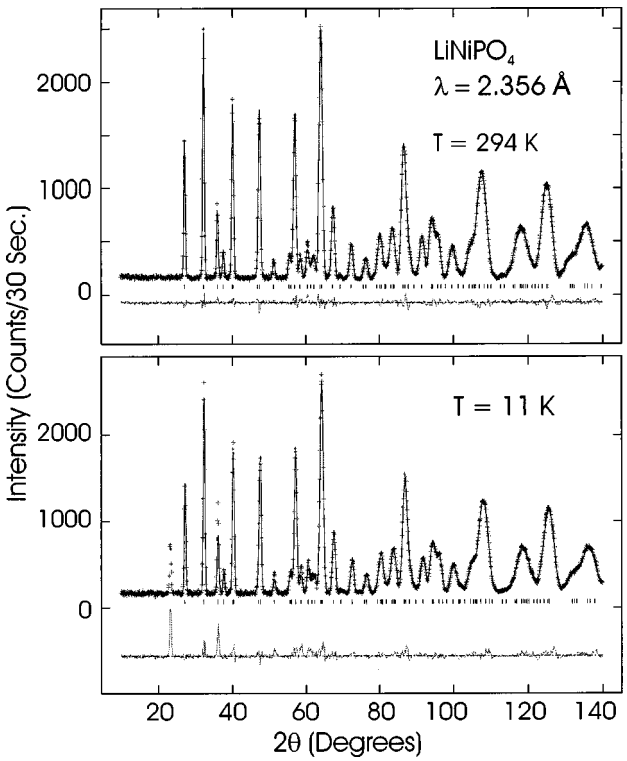

FIG. 1. Neutron powder diffraction patterns at 10 K and at 294 K of $LiNiPO_4$. The solid lines are fits to the data using *Pnma* symmetry with the structural parameters in Table I; the lower dashed line is the difference between the measured (+ symbols) and the fitted curve.

III. RESULTS AND DISCUSSION

A. Two-dimensional antiferromagnetism in pure $LiNiPO_4$

1. Neutron diffraction

To determine the purity of the sample and the variations upon cooling below room temperature, neutron powder diffraction patterns were collected in the 2θ range 10°-140° at 294 K and 10 K. The structure was refined using the Rietveld method with the GSAS program.[16] The structural parameters of $LiNiPO_4$ determined by Geller and Duran[17] and refined by Abrahams and Easson[18] were used as initial parameters for the fitting. Due to the presence of Li in the sample, absorption corrections were calculated and accounted for in the analysis.[16] Figures 1(a) and 1(b) show the diffraction patterns at 10 K and 294 K for $LiNiPO_4$. The cell dimensions and atomic positions, listed in Table I, are consistent within error with those determined by Abrahams and Easson.[18] The thermal factor for Li is much higher than that of other atoms as expected for a lighter and smaller ion.

At low temperatures a new set of reflections, which can be indexed based upon the chemical unit cell, is observed, as is shown in the difference between the calculated fit and the

TABLE I. Structural parameters of $LiNiPO_4$ at $T=10$ K and at $T=294$ K obtained from the diffraction data shown in Fig. 1. The model structure has $Pnma$ symmetry.

Atom	x	y	z	$U\times100$ (Å^2)
		$T=294$ K		
Li	0.0	0.0	0.0	1.8(3)
Ni	0.2761(1)	0.25	0.9812(5)	0.33(7)
P	0.0943(4)	0.25	0.4170(7)	0.20(11)
O(1)	0.0989(4)	0.25	0.7434(8)	0.56(12)
O(2)	0.4522(3)	0.25	0.2019(6)	0.00(11)
O(3)	0.1662(3)	0.0415(4)	0.2773(4)	0.31(7)
$a=10.0927(5)$ Å	$b=5.8905(3)$ Å	$c=4.7050(2)$ Å	Cell volume	$=279.78(2)$ Å^3
		$T=10$ K		
$a=10.0738(10)$ Å	$b=5.8768(5)$ Å	$c=4.6969(4)$ Å	Cell volume	$=278.07(4)$ Å^3

measured data in Fig. 1. To minimize thermal effects, the diffraction pattern was measured at $T=50$ K and subtracted from that measured at $T=5$ K as is shown in Fig. 2. To account for the extra reflections we follow Santoro *et al.*[8–10] in their analysis of the magnetic structure of LiMPO$_4$ compounds and propose that they are due to the AF ordering of Ni^{2+} $(S=1)$. The model is such that Ni^{2+} $(S=1)$ ions located at $[\frac{1}{4}+\epsilon,\frac{1}{4},-\delta]$, $[\frac{1}{4}-\epsilon,\frac{1}{4},\frac{1}{2}-\delta]$ (referred to as sites Ni1 and Ni2) are antiparallel to one another and the ions at $[\bar{\frac{1}{4}}-\epsilon,\bar{\frac{1}{4}},\delta]$, $[\bar{\frac{1}{4}}+\epsilon,\bar{\frac{1}{4}},\frac{1}{2}+\delta]$ (Ni3 and Ni4) are anti-parallel to the first pair, as depicted in Fig. 3. Here $\epsilon=0.026$ and $\delta=0.018$ as determined from the powder diffraction analysis (see Table I). The magnetic model is similar to that of the isostructural compounds LiMPO$_4$ (M=Mn, Fe, Co) but with different spin orientations. The Ni spin system (at positions Ni1 and Ni2; see above) spans a buckled rhombus lattice with an edge length (i.e., nearest-neighbor distance) $a=3.81$ Å and an angle $\alpha\approx101.4°$ (or, equivalently, a centered rectangular lattice with $b=5.8$ Å and $c=4.7$ Å, see Fig. 3). These buckled NiO layers are orthogonal to the a axis and are about 5.0 Å apart. The distance between nearest-neighbor Ni ions in adjacent planes is 5.8 Å. The magnetic structure factor for a general (h,k,l) reflection can be readily calculated on the basis of the magnetic model shown in Fig. 3:

$$F_{\rm Ni}=4\mu_{\rm Ni}f_{\rm Ni}(Q)\sin\left[\pi\left(2h\epsilon+\frac{k}{2}-2l\delta\right)\right]\cos\left(\frac{\pi h}{2}\right)$$

for even l's,

$$4\mu_{\rm Ni}f_{\rm Ni}(Q)\cos\left[\pi\left(2h\epsilon+\frac{k}{2}-2l\delta\right)\right]\sin\left(\frac{\pi h}{2}\right)\quad\text{for odd } l\text{'s},\tag{1}$$

where $f_{\rm Ni}(Q)$ is the magnetic form factor of Ni^{2+} at momentum transfer $Q=2k_0\sin\theta$, and $\mu_{\rm Ni}$ is the average magnetic moment of the Ni^{2+} ion. To extract the average ordered magnetic moment and its direction ($\hat{s}_{\rm Ni}$ is a unit vector in the

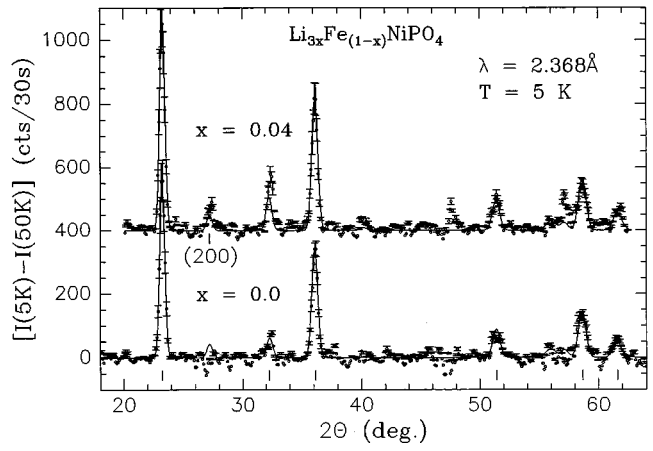

FIG. 2. The difference between diffraction patterns taken at $T=5$ K and $T=50$ K for pure $LiNiPO_4$ (lower part) and impure $(Li_{1-3x}Fe_x)NiPO_4$ (upper part). These extra reflections are due to the antiferromagnetic ordering of the Ni^{2+} spins $(S=1)$ and can be indexed based on the chemical unit cell. The solid lines are the best fits to the data with the AF models as described in the text. Notice that the (200) magnetic reflection is stronger for the impure sample (upper curve), indicating stronger couplings between the planes when Fe is inserted into $LiNiPO_4$.

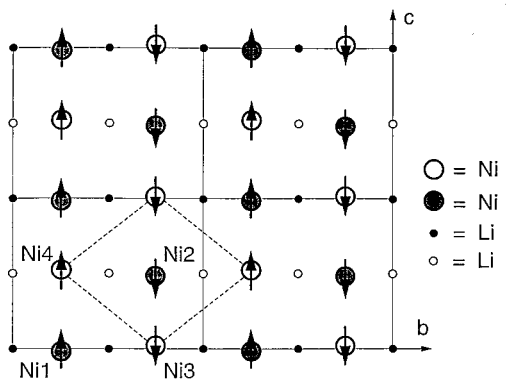

FIG. 3. Depiction of the magnetic structure model of $LiNiPO_4$, showing the projection of four unit cells onto the b-c plane (phosphorous and oxygen atoms are omitted). The Ni atoms form two antiferromagnetic buckled layers that are orthogonal to the a axis at $x=\frac{1}{4}$ (solid circles) and at $x=\frac{3}{4}$ (open circles), where x represents the fractional position along the a axis. Dashed line rhombus shows the 2D magnetic unit cell. Li atoms form flat layers at the $x=0$ (solid circles) and at $x=\frac{1}{2}$ (open circles).

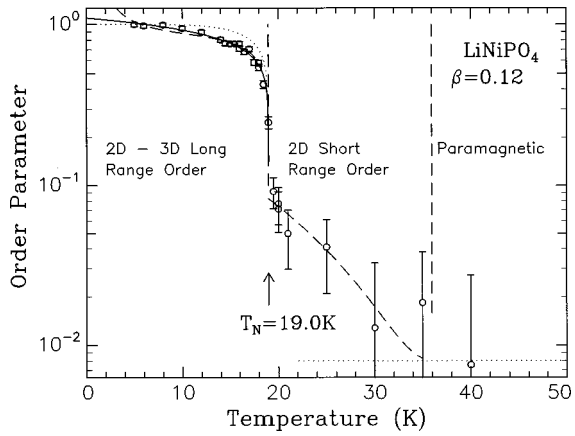

FIG. 4. The normalized intensity of the (010) AF reflection vs temperature T. The solid line is a fit to the power law function, Eq. (3), yielding a $T_N=19.1\pm0.5$ K and $\beta=0.12\pm0.01$. The dotted and dashed lines are fits to the data using the staggered magnetizations $M^{\dagger}_{2D}(T)$ and $M^{\dagger}_{CO}$, respectively, as discussed in the text. Above T_N elastic scattering is observed due to the finite correlations in the 2D system. Below T_N the magnetic system has long-range 2D order with weak interplanar correlations, above T_N the system has short range 2D correlations, and for $T\geqslant 40$ K the magnetic system is in the paramagnetic phase.

direction of the moment), the magnetic diffraction data in Fig. 2 are fitted to the calculated intensity[19]

$$I=\frac{A[F_{\mathrm{Ni}}(\hat{s}_{\mathrm{Ni}}-\hat{s}_{\mathrm{Ni}}\cdot\hat{\kappa})r_0]^2}{\sin(\theta)\sin(2\theta)}, \tag{2}$$

where A is a known scale factor determined from the fitting procedure to the nuclear diffraction pattern (Fig. 1), $\hat{\kappa}$ is a unit vector in the direction of the scattering vector ($\mathbf{Q}=\mathbf{k}_i-\mathbf{k}_f$), and $r_0=0.269\times10^{-12}$ cm. Four adjustable parameters were refined in the fitting procedure: the magnitude of the average magnetic moment μ_{Ni}, the angle ϕ that the magnetic moments make with respect to the c axis in the a-c crystallographic plane[20] ($\cos\phi=\hat{s}_{\mathrm{Ni}}\cdot\hat{\kappa}$), and two global peak-shape parameters. The magnetic Bragg peaks are assumed to be of Gaussian shape with a width Δ that varies linearly with the scattering angle 2θ as $\Delta(2\theta)=\Delta_0+2\theta\Delta_1$ over the 2θ range shown in Fig. 2. The solid line in Fig. 2 is the best fit to the experimental data, yielding an angle $\phi=0\pm3°$; i.e., the magnetic moment points in the c-axis direction. The extracted average magnetic moment $gS=(2.83\pm0.1)\mu_B$ per Ni atom. The (200) magnetic reflection (at $2\theta_{(200)}=27.24°$; see Fig. 2) is weaker in intensity than the model predicts, indicative of poor correlations between the magnetic planes, even at temperatures as low as 2 K.

Figure 4 shows the normalized integrated intensity $I(T)$ of the (010) reflection as a function of temperature. The intensity of the magnetic peak depends on the AF staggered magnetization $I(T)\sim|M^{\dagger}(T)|^2$, which is also the order parameter of the magnetic system. As a first step in the characterization of the spin system (spin symmetry, in particular), we assume a power law function for the order parameter

$$M^{\dagger}(T)/M^{\dagger}(0)=A(1-T/T_N)^{\beta}, \tag{3}$$

which yields a $\beta=0.12\pm0.01$ and a Néel temperature $T_N=19.1\pm0.5$ K. The value of the critical exponent β is consistent with the layered nature of the spin system and, in fact, is very close to the exact theoretical value of the 2D square Ising model ($\beta=0.125$).[21] Similar observations concerning layered Ni^{2+} in other systems have been reported.[22] In particular, in the case of K_2NiF_4, despite the fact that the spin Hamiltonian is isotropic, additional weak anisotropy dominates the behavior at the critical region, giving rise to a $\beta=0.14$ (Ref. 23).

To construct a Hamiltonian for the spin system we recall that the in-plane superexchange interaction of nearest neighbors in $LiNiPO_4$, J_{2D}, through the Ni-O-Ni path is expected to be much stronger than that between nearest interplane neighbors, $J_{\perp}$, with a Ni-O-P-O-Ni path, which is of a higher-order perturbation.[11] These couplings are generally isotropic where anisotropic terms are usually very small. Here we argue that the Ising-like behavior is invoked by a local perturbation term of the form $-D(S^z)^2$ due to crystal field effects and spin-orbit coupling.[24] This term is common to transition-metal ions in an axial or rhombic symmetry (Refs. 25–28) which, for Ni^{2+}, leads to a zero-field splitting of the triplet, into a doublet and a singlet. With the above-mentioned arguments we propose the following spin Hamiltonian for this highly anisotropic magnetic system:

$$\mathcal{H}=\sum_{\mathrm{r}}\left[-\mathrm{J}_{2\mathrm{D}}\sum_{\mathrm{j}}\mathrm{S}_{\mathrm{r}}\cdot\mathrm{S}_{\mathrm{r+j}}-J_{\perp}\sum_{\mathrm{l}}\mathrm{S}_{\mathrm{r}}\cdot\mathrm{S}_{\mathrm{r+l}}-D(S^z_{\mathrm{r}})^2\right], \tag{4}$$

where r labels the Ni spins in the 3D structure, and j labels the four in-plane and l labels the interlayer nearest-neighbor Ni sites. For $D>0$ the ground state of the spin system is doubly degenerate and the only transformation that leaves the ground state invariant is the one in which $S^z_{\mathrm{r}}\rightarrow-S^z_{\mathrm{r}}$. According to the universality hypothesis,[29] the critical behavior of a spin system is dominated by the ground state of the free spin, and thus, by virtue of the zero-field-splitting term, the Ni^{2+} spin system resembles that of the $S=\frac{1}{2}$ Ising model for which the spontaneous staggered magnetization is given by[21]

$$M^{\dagger}_{2D}(T)=M^{\dagger}(0)[1-\sinh^{-4}(2\tilde{J}_{2D}/T)]^{1/8}, \tag{5}$$

where $\tilde{J}_{2D}$ is an effective Ising coupling. Although close to the transition temperature, Eq. (5) fits the order parameter, with $\tilde{J}_{2D}=-8.4$ K reasonably well (dotted line Fig. 4), a significant difference between the measured and calculated order parameter is observed at lower temperature ($T<T_N$). This deviation, as we argue below, is due to the spatial crossover from the 2D to the 3D ordering caused by the weak interlayer nearest-neighbor average coupling ($\tilde{J}_{\perp}$). Just below the onset of the 2D long-range order, the interaction between staggered magnetizations of adjacent layers (after renormalization of the exchange) can be approximated by the 1D Ising model. Although the 1D system does not order at any finite temperature, the magnetization at zero magnetic field and the correlation length grow exponentially as the temperature is lowered as $M_{1D}\sim e^{2\tilde{J}_{\perp}/T}$. Therefore, in this approximation the order parameter in the crossover from 2D to 3D, Eq. (5), is modified to

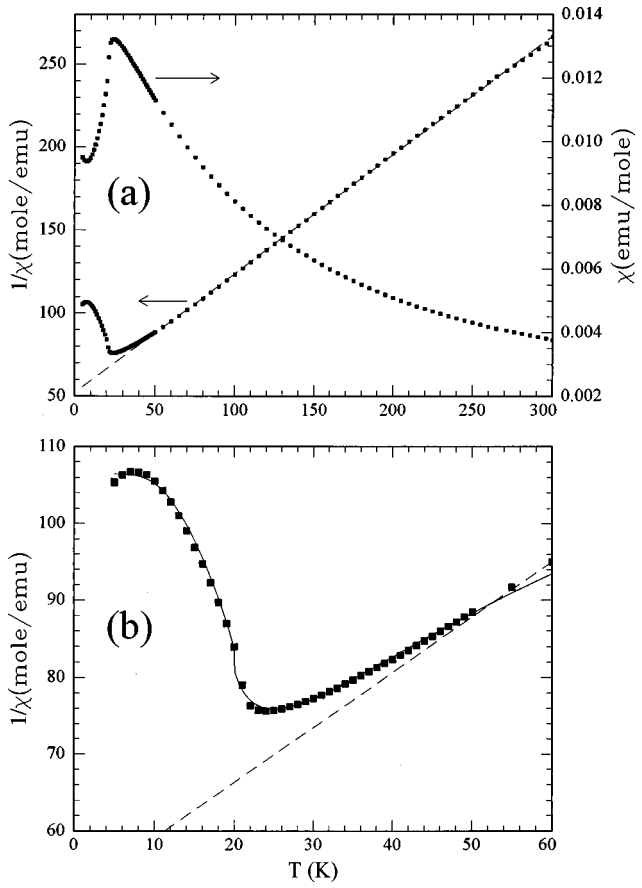

FIG. 5. (a) Magnetic susceptibility and its inverse versus temperature for $LiNiPO_4$. The linear fit to the data (dashed line) in the paramagnetic regime (50–300 K), is the Curie-Weiss law with an effective magnetic moment of $g\sqrt{S(S+1)}=(3.2\pm0.1)\mu_B$. (b) Inverse magnetic susceptibility in the vicinity of the antiferromagnetic transition. The solid line is a linear combination of the parallel and perpendicular susceptibilities of the plane square Ising model.

$$M^{\dagger}_{\mathrm{CO}}(T)\sim e^{2\tilde{J}_{\perp}/T}M^{\dagger}_{\mathrm{2D}}(T). \tag{6}$$

Fitting the measured intensity in Fig. 4 with Eq. (6) (although it fails at very low temperatures $T\leqslant 4$ K) yields $\tilde{J}_{\mathrm{2D}}=-8.4\pm0.2$ K and $\tilde{J}_{\perp}=-0.4\pm0.02$ K.

At temperatures $T\geqslant T_N$ the magnetic scattering persists in the form of diffuse scattering to almost $2T_N$ before reaching the background level. Such quasielastic scattering at the nominal (010) is due to the finite integration of the resolution function of the spectrometer over the scattering along the (h00) *rod*, originating from the 2D short-range order above T_N. Such behavior is characteristic of the 2D Ising model where the correlation length remains finite up to about $T\sim 2T_N$ (Ref. 21).

2. Magnetic susceptibility

The magnetic susceptibility versus temperature $\chi(T)$, for pure $LiNiPO_4$, was measured in the temperature range 4–300 K, as shown in Fig. 5, and was found to be practically independent of magnetic field (up to $H=5$ T) except for a very subtle field dependence at very low temperatures, as discussed below. The inverse magnetic susceptibility $1/\chi(T)$ shown in Fig. 5 is linear in the temperature range 50–300 K, characteristic of a paramagnetic system, with a broad minimum at $T_m\approx 22$ K, indicating an AF transition. Using the Curie-Weiss law $\chi(T)=C/(T+\theta)$ and $C=N_A(g\mu_B)^2S(S+1)/3k_BT$ to fit to the measured inverse susceptibility $1/\chi(T)$ (dashed line in Fig. 5) yields an effective moment $\mu=(3.2\pm0.1)\mu_B$ ($g=2.26$) and $\theta=74\pm2$ K. Similar results are also obtained from the exact treatment of the spin Hamiltonian in the molecular field (MF) approximation as shown below. At high temperatures $T\gg J_{\mathrm{2D}}$ (and neglecting the interlayer exchange $J_{\perp}$), the Hamiltonian in Eq. (4) can, in the MF approximation, be written as follows:

$$\mathcal{H}=-g\mu_B\left[H_z^{\mathrm{eff}}S_z+\frac{1}{2}(H_+^{\mathrm{eff}}S_-+H_-^{\mathrm{eff}}S_+)\right]-DS_z^2, \tag{7}$$

where $\mathbf{H}^{\mathrm{eff}}=\lambda\mathbf{M}$; $\lambda=J_{\mathrm{2D}}(g\mu_B)^2N_A)/z$ ($\mathbf{M}$ is the magnetization, $z=4$ is the number of in-plane NN's, and $H_{\pm}=H_x\pm iH_y$, $S_{\pm}=S_x\pm iS_y$). In the MF approximation $\chi^{\alpha}(T)=\chi_0^{\alpha}/(1-\lambda\chi_0^{\alpha})$, where χ_0^{α} is the free spin susceptibility in the absence of exchange with the magnetic field parallel and perpendicular ($\alpha=\parallel$ and $\perp$, respectively) to the quantization axis. It is then calculated in the usual way:

$$\chi_0^{\alpha}(T)=\frac{N_A}{ZH_{\alpha}}\sum_i\frac{-dE_i^{\alpha}}{dH_{\alpha}}e^{E_i^{\alpha}/T},$$

where Z is the partition function. The energy levels in the absence of an exchange interaction ($\lambda=0$), E_i^{α}, can be obtained by diagonalization of the 3×3 matrix associated with Eq. (7), in particular, for $H_{\parallel}$,

$$E^{(\pm1)}=-D\mp g\mu_BH_{\parallel},\quad E^{(0)}=0, \tag{8}$$

and for $H_{\perp}$,

$$E^{(\pm1)}=-\frac{D}{2}\mp\sqrt{\frac{D^2}{4}+(g\mu_BH_{\perp})^2},\quad E^{(0)}=-D. \tag{9}$$

Equations (8) and (9) show that at zero magnetic field the triplet is split into a singlet and a ground state doublet. Using this procedure to fit the susceptibility in the temperature range 50–300 K yields $g=2.36\pm0.02$, $J_{\mathrm{2D}}=26\pm3$ K, and provides only an upper limit to the absolute value of the zero-field splitting, $|D|<25$ K.

In accordance with the neutron scattering analysis and the topology of the Ni planes, we assume that the appropriate model to characterize the system in the temperature range 4–50 K is the square lattice Ising antiferromagnet, with the simplified Hamiltonian

$$\mathcal{H}=-\tilde{J}_{\mathrm{2D}}\sum_{(i,j)}S_i^zS_j^z-g\mu_BH_z\sum_iS_i^z-g\mu_BH_x\sum_iS_i^x, \tag{10}$$

where the interactions of spins with the magnetic fields along and perpendicular to the axis of quantization are also included. The properties of the Hamiltonian (10) for a variety of lattices were thoroughly investigated[30] and are well understood now. The parallel susceptibility $\chi_{\parallel}(T)$ for the plane-square antiferromagnet was calculated by Sykes and Fisher[31] using the series expansions method. Their calculation of $\chi_{\parallel}(T)$ is given in terms of two sets of series, one for temperatures $T\geqslant T_N$ [Eq. (5.18), Ref. 31] and the other for T

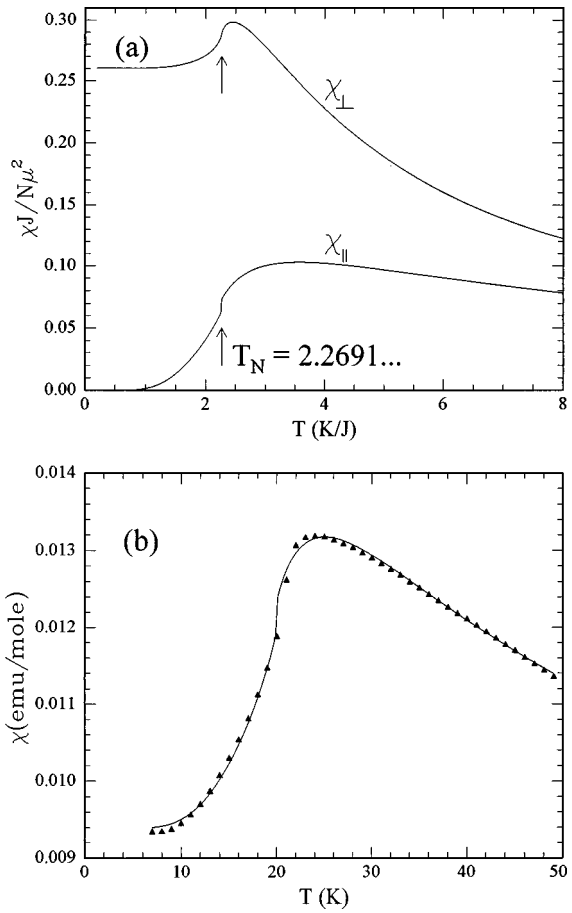

FIG. 6. (a) Parallel and perpendicular susceptibilities [$\chi_\parallel(T)$ and $\chi_\perp(T)$, respectively] of the plane-square lattice Ising antiferromagnet as calculated in Refs. 31 and 32. (b) Magnetic susceptibility of $LiNiPO_4$ at low temperatures. The solid line is a fit to the data using a linear combination of the aforementioned parallel and perpendicular susceptibilities as follows: $\chi(T)=a\chi_\parallel(T)+b\chi_\perp(T)+c$.

$\leqslant T_N$ [Eq. (6.7), Ref. 31], as reproduced in Fig. 6(a). The perpendicular susceptibility $\chi_\perp(T)$ corresponding to the Hamiltonian (10) for the plane square was solved exactly by Fisher.[32] Figure 6(a) shows $\chi_\perp(T)$ for the plane-square antiferromagnet as calculated by using Eq. (5.42) of Ref. 32. The Ising-like behavior of the Ni^{2+} spins in $LiNiPO_4$ ($S=1$), as argued above, is by virtue of the zero-field splitting that creates a ground state doublet that is separated from other excited states by an energy gap of at least D. This picture is true for both fields parallel and perpendicular to the axis of quantization. However, the calculation of the susceptibility involves first and second derivatives of energy levels with respect to the magnetic field, and those in the present case differ for parallel and perpendicular fields. For the parallel susceptibility, the energy levels are linear in a magnetic field, Eq. (8), as for the spin $S=\frac{1}{2}$ system, and therefore the calculations of Sykes and Fisher apply exactly. However, in the case of perpendicular fields, the ground state doublet splits into an energy level that is quadratic in field and another that is a constant, Eqs. (9). We argue that qualitatively, the general form of $\chi_\perp(T)$ will resemble that of the spin $S=\frac{1}{2}$ model,[32] although it might be significantly reduced in amplitude. To model the measured susceptibility from our polycrystalline $LiNiPO_4$ sample at low temperatures, a linear combination of the two susceptibilities is constructed as follows:

$$\chi(T)=A\chi_\parallel(T)+B\chi_\perp(T)+C, \tag{11}$$

where A, B, and C are constants to be determined from the fit to the data. The solid line in Fig. 6(b) represents the best fit to the data as measured at $H=1000$ G, using Eq. (11) with $J=-8.83\pm0.1$ K ($T_N=20.0\pm0.25$ K) and $A=0.0350\pm0.0004$, $B=0.0142\pm0.0002$, and $C=0.0057\pm0.0005$ all given in units of emu/mol. Ideally, for the spin $S=\frac{1}{2}$ system, the ratio $A/B=\frac{1}{2}$; however, experimentally a ratio $A/B=2.47\pm0.07$ (for $H=1000$ G) is obtained, indicating that the susceptibility of the polycrystalline sample is dominated by the parallel component of Eq. (11) consistent with the discussion above. The A/B ratio was also extracted at various magnetic fields, as shown in Table II. The gradual increase in the contribution of $\chi_\perp(T)$ as the field is increased is in qualitative agreement with the field dependence of the energy levels in Eq. (9). Even at magnetic fields as high as $H=50\,000$ G, $\chi_\parallel(T)$ dominates the susceptibility, and that allows us to estimate a lower limit for D from Eq. (9): $D>2g\mu_B H\approx13$ K. Single-crystal studies of $LiNiPO_4$ and exact determination of the parallel and perpendicular susceptibility might shed more light on this problem, but this is not available to us at this time.

TABLE II. The ratio A/B, where A and B are the constants used in Eq. (11) and determined from the fit to the susceptibility data for the polycrystalline $LiNiPO_4$ at various magnetic fields. The decrease in the ratio at high fields is in qualitative agreement with the energy levels being quadratic in the field due to the zero-field-splitting term D. See text for more details.

H (G)	A/B
50	2.52(7)
1000	2.47(6)
50000	2.30(5)

B. Iron-impurity-induced three-dimensional antiferromagnetism in $(Li_{0.90}Fe_{0.033})NiPO_4$

1. Neutron diffraction

Structural analysis of the doped compound ($x=0.033$) indicates that $Pnma$ symmetry is preserved upon substitution of Li sites with Fe as is demonstrated in Fig. 7 and Table III. The integration of iron into Li positions does not disrupt the structure and does not introduce new phases. At higher iron concentrations ($x\geqslant0.04$) the compound consists of $(Li_{1-3x}Fe_x)NiPO_4$ and an additional well-defined $Li_3Fe_2(PO_4)_3$ phase.[33] A significant change in the thermal factor of Li is observed (compare Tables I and III), indicating a more localized Li in the impure compound. The low-temperature data (see Figs. 2 and 7) show magnetic reflections that are similar to those of the pure compound although they differ in their relative intensities. The magnetic (200) reflection, which was found to be very weak for the pure $LiNiPO_4$, is more prominent in the impure compound, indicating stronger correlations between planes. In addition to the AF magnetic peaks, weak reflections superimposed on

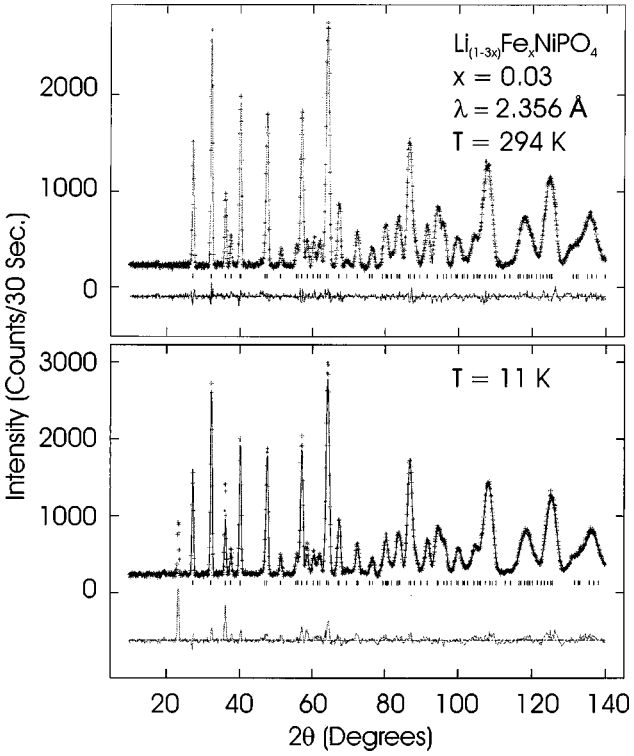

FIG. 7. Neutron powder diffraction patterns at 10 K and 294 K of $(Li_{1-3x}Fe_x)NiPO_4$. The solid lines are fits to the data using the *Pnma* symmetry with the structural parameters listed in Table II; the lower dashed line is the difference between the measured (+ symbols) and the fitted curve.

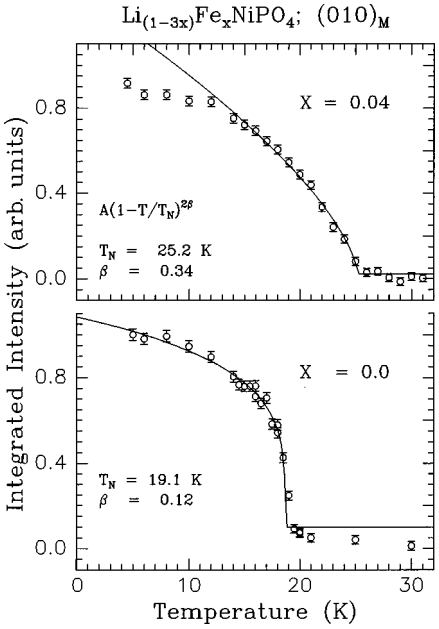

FIG. 8. Normalized intensities of the (010) AF reflection for the pure (upper part) and for the impure compounds (lower part), demonstrating the effect on T_N and on the temperature dependence of the order parameter as the system is doped with iron.

nuclear Bragg reflections are observed, indicating the presence of a ferromagnetic component in this system. The most intriguing feature of our results is the behavior of the order parameter as a function of temperature as measured on the lowest-order AF Bragg reflection (010). Figure 8 shows the order parameters of the pure and doped samples, demonstrating that insertion of iron into the pure $LiNiPO_4$, even in this minute amount, modifies the critical behavior significantly. It drives the AF transition to a higher temperature, from $T_N = 19.1 \pm 0.5$ K to $T_N = 25.2 \pm 0.5$ K, and changes the critical exponent from $\beta = 0.12 \pm 0.01$ to $\beta = 0.34 \pm 0.02$. In addition, it should be noted that the AF transitions for the pure and impure compounds are remarkably sharp with no indications of smeared Néel temperatures as observed for K_2NiF_4 or the random site $Rb_2(Mn_{0.5}Ni_{0.5})F_4$ (see, for instance, Fig. 2 in Ref. 23). In these compounds, it was found that the smearing of the transition increases approximately proportionally with the length of the crystals along the *c* axis regardless of impurities.

To account for the extra reflections we propose a noncollinear model (see Fig. 9) with a simple modification of the magnetic structure factor of the pure $LiNiPO_4$ compound (derived in the previous section), as follows:

$$F_M \sim F_{\mathrm{Ni}}[\hat{s}_{\mathrm{Ni}} - (\hat{\kappa}\cdot\hat{s}_{\mathrm{Ni}})\hat{\kappa}] + wF_{\mathrm{Fe}}[\hat{s}_{\mathrm{Fe}} - (\hat{\kappa}\cdot\hat{s}_{\mathrm{Fe}})\hat{\kappa}], \tag{12}$$

TABLE III. Structural parameters of $(Li_{1-x}Fe_x)NiPO_4$ at $T = 10$ K and at $T = 294$ K obtained from the diffraction data shown in Fig. 7. The space group of the doped compound is the same as that of the pure $LiNiPO_4$ compound (*Pnma*) with no indications of any structural phase transitions.

		$T = 294$ K		
Atom	*x*	*y*	*z*	$U \times 100$ Å^2
Li (0.94)	0.0	0.0	0.0	1.0(6)
Fe (0.03)	0.0	0.0	0.0	1.0(6)
Ni	0.2762(2)	0.25	0.9824(6)	0.6(1)
P	0.0954(4)	0.25	0.4192(9)	0.3(1)
O1	0.1018(5)	0.25	0.742(1)	0.2(1)
O2	0.4540(4)	0.25	0.1983(8)	0.2(1)
O3	0.1661(3)	0.0415(5)	0.2767(6)	0.38(9)
$a = 10.0832(6)$ Å	$b = 5.8836(3)$ Å	$c = 4.7147(2)$ Å	Cell volume	$= 279.703(26)$ Å^3
		$T = 10$ K		
$a = 10.0652(10)$ Å	$b = 5.8692(5)$ Å	$c = 4.7048(4)$ Å	Cell volume	$= 277.93(4)$ Å^3

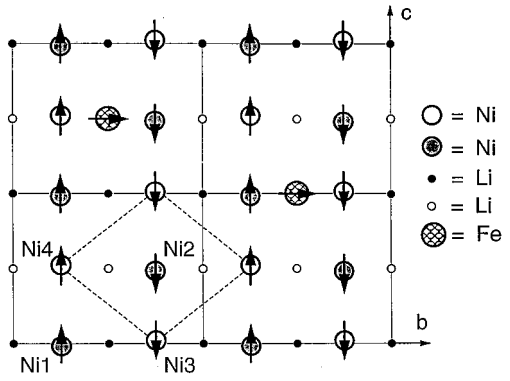

FIG. 9. Modified magnetic model structure for the iron-substituted compound $(Li_{1-3x}Fe_x)NiPO_4$. Iron occupies random Li sites between antiferromagnetic layers (as described in more detail in the caption of Fig. 3). The iron moments couple antiferromagnetic Ni layers, driving the Néel temperature to higher values, and modify the characteristics of the transition. The fit to the magnetic diffraction data in Fig. 2 suggests that iron moments are pointing in a direction perpendicular to that of Ni moments. Such a preferred orientation for iron can be due to an anisotropic exchange interaction of the form $J\mathbf{S}_{Fe}\times\mathbf{S}_{Ni}$ or due to frustration. The frustration arises because Fe, by symmetry, interacts identically with its two nearest-neighbor Ni moments (in adjacent layers) which in the pure system align antiparallel to one another.

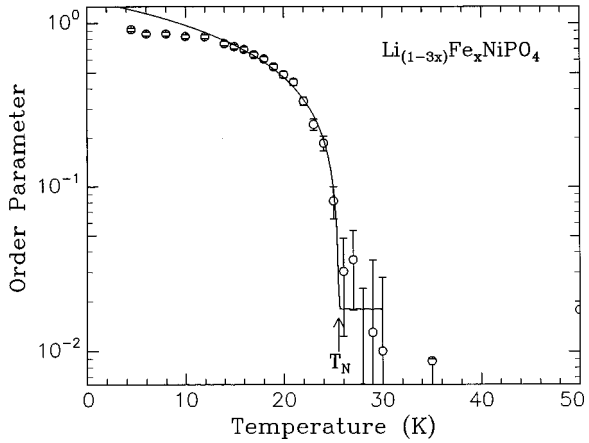

FIG. 10. The normalized intensity of the (010) AF reflection versus temperature for the impure compound. The solid line is a fit to the power law function, Eq. (3), yielding a $T_N=25.2\pm0.2$ K and $\beta=0.34\pm0.02$. Unlike the case of the pure system, the 2D critical scattering is practically suppressed above T_N.

where F_{Ni} is given by Eq. (1), w is a weight factor fixed by the fraction of iron present in the compound, and $F_{Fe}=f_{Fe}(Q)\mu_{Fe}$. For simplicity, it is assumed that the Fe^{3+} ion is present at the origin of the chemical unit cell, replacing Li, with an occupation factor that is consistent with its presence in the compound. There are five adjustable parameters in this model, the average magnetic moments μ_{Ni},μ_{Fe}, the angle ϕ_{Fe} that the iron magnetic moment makes with the b axis in the b-c crystallographic plane, and two additional parameters for the peak-shape function, as discussed in the previous section. The direction of the Ni moment was fixed along the c axis, just as it is in the pure compound. The fit of Eq. (12) to the data shown in Fig. 2 (upper part) is best when the magnetic moment of the iron is pointing at an angle $0\pm10°$ away from the b axis, i.e., orthogonal to the direction of the magnetic moments of the Ni system, creating a noncollinear magnetic system. The average magnetic moments are $\mu_{Ni}=(2.8\pm0.1)\mu_B$ per Ni and $\mu_{Fe}=5.9\pm1$ per Fe atom. Such a noncollinear arrangement of the mixed spin system can be due to an asymmetric Ni-Fe exchange of the form

$$-J_{\text{Fe-Ni}}\mathbf{S}_{Ni}\times\mathbf{S}_{Fe}, \tag{13}$$

which tends to align the spins perpendicular to one another. Alternatively, in the case of isotropic interaction with nearby Ni ions, it can be the result of *frustration* that an Fe moment experiences. The frustration arises because, by symmetry, Fe interacts identically with its two nearest-neighbor Ni moments in adjacent layers. Below the AF transition, these two Ni moments align antiparallel to one another, and thus if the in-plane collective forces are strong enough to hold them antiparallel, the net interaction with the iron will cancel out and it will be *frustrated*. Such an effect will lead to spin-glass-like behavior of the Fe magnetic subsystem for $T<T_N$, as evidenced in the susceptibility measurements discussed below. In the other extreme of very weak coupling between layers, as in the paramagnetic state, the effective interaction between the two NN Ni moments in adjacent layers (embracing an Fe) is *ferromagnetic* (FM) regardless of the type Fe-Ni coupling, i.e., AF or FM. We thus expect the iron moment to destroy correlations in the plane above T_N. This is consistent with the absence of diffuselike scattering above the transition as is shown in Fig. 10, and in contrast to the observation for the pure compound (compare with Fig. 4 of the pure compound). It is therefore surprising that, despite the fact that iron moments couple adjacent planes at random sites, not in accordance with the natural interlayer coupling of the pure compound (introducing *frustration*), their intercalation induces an AF transition at a significantly higher temperature.

2. Magnetic susceptibility

Figure 11 shows the susceptibility of $(Li_{0.90}Fe_{0.033})NiPO_4$ (and its inverse) measured under 50 G (triangles) and 1000 G (squares), indicating strong field-dependent effects at low temperatures. At temperatures $T>30$ K the susceptibility is independent of applied magnetic field within error, and its inverse is linear in T, indicating that in this T range the system is paramagnetic. From the fit of $1/\chi(T)$ to the Curie-Weiss law we obtain an effective moment $\mu_{eff}=(2.96\pm0.05)\mu_B$ per Ni and $\theta=100.8\pm2$ K. Two field-dependent maxima at $T_{m1}=12$ K and $T_{m2}=28$ K are observed in the susceptibility. It is most striking that paramagnetic behavior persists down to temperatures that are very close to the transition temperature, with no clear indication of the transition which occurs at $T_N=25.2\pm0.5$ K. By contrast, the behavior of pure $LiNiPO_4$ is completely different, with a gradual deviation from pure paramagnetism at $T\geqslant2T_N\sim50$ K. This is consistent with our assertion that the Fe moments tend to create local frustration between adjacent layers. And it is also consistent with the absence of diffuselike neutron scattering of the order parameter (Fig. 10).

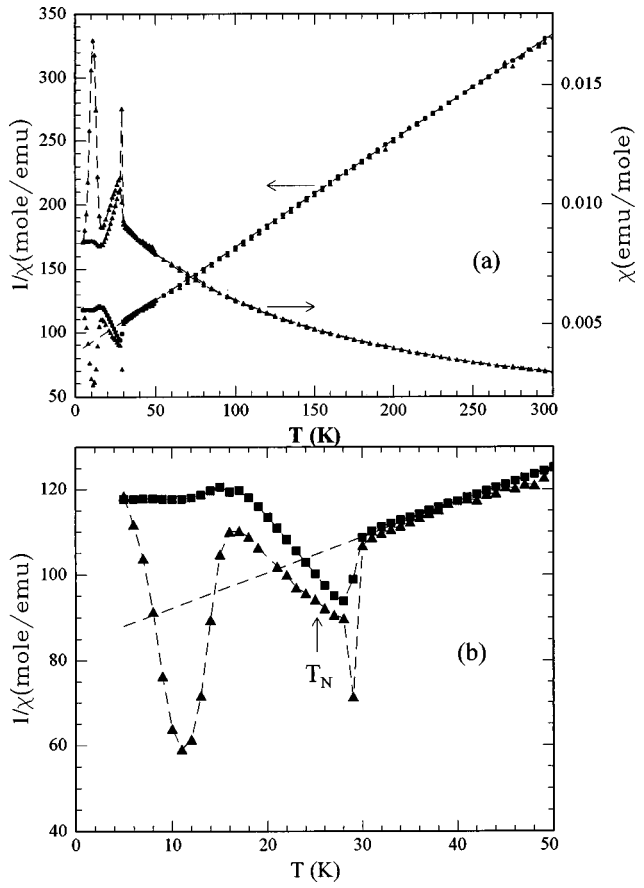

FIG. 11. (a) Magnetic susceptibility and its inverse versus temperature for $(Li_{1-3x}Fe_x)NiPO_4$. The linear fit to the data (dashed line) in the paramagnetic regime (50–300 K) is the Curie-Weiss law with an effective magnetic moment $\mu=(2.96\pm0.1)\mu_B$, and $\theta=100.8\pm2$. (b) Inverse magnetic susceptibility in the vicinity of the antiferromagnetic transition showing a magnetic field dependence characteristic of spin glass behavior. Magnetic susceptibilities were meausred under 50 G (triangles) and under 1000 G (squares).

The placement of an Fe ion in a Li site can affect the magnetic state of Ni in at least two ways. First, the Fe moment can couple magnetically via superexchange or direct exchange interaction with Ni ions of adjacent layers. In addition, it can modify the charge distribution around the nearby Ni; in particular it can distort the crystal field around the ion. Fe, with an effective charge that is 3 times that of Li, will lower the symmetry of charge around Ni, and that together with spin-orbit coupling can significantly enhance the zero-field-splitting term or even introduce other terms that will split all the levels of the spin $S=1$ (Ref. 25). The local spin Hamiltonian for Ni in the vicinity of an Fe impurity can thus be of the form[25]

$$\mathcal{H}=\mathbf{S}_{\mathrm{Fe}}\mathbf{J}\mathbf{S}_{\mathrm{Ni}}+g\mu_B\mathbf{H}\cdot\mathbf{S}_i-D(S_z)^2-E(S_x^2-S_y^2), \quad (14)$$

where **J** is a tensor and the term involving E is the result of symmetry that is lower than axial or tetragonal (rhombic). Diagonalization of the matrix associated with Eq. (14) gives three distinct energy levels even in the absence of magnetic field. This means that the ground state of the free Ni spin near an iron can be singlet with a moment pointing in a certain direction. The many-body Hamiltonian for the doped system is thus much more complicated and can probably be simplified in such a way as to belong to the class of layered planar Ising (LPI) models.[38] A layered Ising model is defined in such a way that in one spatial dimension the coupling is random, whereas in the other dimensions (2D in this case) the coupling is of the same strength.

Figure 11 shows a deviation from linearity in $1/\chi(T)$ below $T\approx30$ K that is very different from the behavior of the pure compound at this T range. Whereas for the pure compound $1/\chi(T)$ indicates increased AF correlations, the deviation from linearity for the impure compound is suggestive of increased FM correlations. This ferromagneticlike behavior above T_N is consistent with the tendency of iron to orient its NN Ni neighbors ferromagnetically as discussed above. The first and second minima in the inverse susceptibility above and below the transition, respectively, depend on the magnetic field in a manner that resembles spin glass systems. This is not surprising in view of the *frustration* in the vicinity of an iron impurity. Neutron scattering under a magnetic field and systematic succeptibility studies are under way to shed light on this behavior.

IV. CONCLUSIONS

Using neutron diffraction experiments in conjunction with magnetic susceptibility measurements we demonstrated that Ni^{2+} moments $(S=1)$ in $LiNiPO_4$ constitute an almost ideal 2D Ising antiferromagnet model. In addition to observing an order parameter that is characteristic of the plane-square Ising system, the weak scattering of the (200) magnetic Bragg reflection is evidence to the poor correlations between the AF planes. The two-dimensional behavior of the spin system is not surprising because, as expected, the Ni ions form layers where nearest neighbors in the plane are coupled via the superexchange Ni-O-Ni and nearest interlayer neighbors are coupled via a much longer Ni-O-P-O-Ni path which is of a higher-order perturbation and therefore much weaker than the in-plane coupling. The in-plane superexchange can in general be isotropic with very weak anisotropies that can assist in a crossover of spin symmetry: from Heisenberg-like to XY or Ising-like behavior. Herein, we have argued that the main mechanism invoking Ising-like properties is a common local zero-field-splitting term, that splits the $S=1$ triplet into a singlet and ground state doublet, with an effective spin $S=\frac{1}{2}$. It is by virtue of the zero-field-splitting term that we could employ well-established results for the Ising model to $LiNiPO_4$. To our knowledge, there is no measurement of the zero-field-splitting term D in this compound; however, the preponderance of experimental evidence is that the larger the distortion of charge symmetry around Ni^{2+} from cubic symmetry,[25–28] the larger this term becomes. Based on careful electron paramagnetic resonance (EPR) measurements[14] of $LiNiPO_4$, and on our susceptibility measurements, we estimate $D>10$ K.

The magnetic susceptibility below and above the AF transition can be fully explained in terms of the pure square 2D Ising model as solved in the seminal works of Fisher and Sykes.[31,32] The fit to the susceptibility data, not just near the critical point, but above and below the transition, is remarkable. The evidence for AF correlations above T_N implicit in

the susceptibility measurements is corroborated by the observation of neutron diffuse scattering at a similar temperature range.

There are very few compounds that exhibit 2D Ising-like behavior, the most important of which is K_2CoF_4 where the $Co^{2+}(3d^7)$ configuration with an effective spin of $S=\frac{3}{2}$ has a ground state doublet (effective $S=\frac{1}{2}$) due to crystal field effects and spin-orbit coupling.[25] Susceptibility measurements near the critical point on single-crystal K_2CoF_4 by Breed *et al.*[34] were found to be in excellent agreement with calculations made by Fisher.[32] Subsequent neutron scattering experiments[35,36] confirmed the 2D Ising-like behavior of this system. However, to our knowledge, the present study provides the first demonstration of Ising-like behavior of Ni^{2+} ($S=1$), and we believe that this is by virtue of the strong zero-field-splitting term in $LiNiPO_4$.

The behavior of the iron-doped compound is much more complicated than that of the pure $LiNiPO_4$, and as we currently lack a rigorous theory, the discussion has been mostly qualitative, based on comparisons with the pure compound. Indeed, the structural and magnetic studies of the pure $LiNiPO_4$ compound proved to be quite important for this qualitative understanding of the doped sample. The two-dimensional characteristics of the pure system seem to be strongly modified by the introduction of minute amounts of iron into the compound. The value of the exponent for the doped compound $\beta=0.34$ is much closer to that of the simple cubic (3D) Ising model $\beta=0.324$ (Ref. 37). The AF transition temperature T_N is increased from $T_N=19.1\pm0.5$ K to $T_N=25.2\pm0.5$ K, indicating stronger coupling between the planes. We argued that an Fe that occupies a Li site can affect the magnetic state of nearby Ni ions in two ways. First, it can magnetically couple via direct or superexchange to a Ni as it is only 3.1 Å apart. Second, the charge difference between Fe^{3+} and the replaced Li^+ can strongly distort the crystal field symmetry around a Ni ion. Such a distortion away from the cubic symmetry enhances the zero-field-splitting term and can introduce other terms that split all three $S=1$ levels.

The Fe ion residing between two Ni ions on adjacent layers (see Fig. 9) effectively couples these two moments ferromagnetically, regardless of the type of Fe-Ni exchange (FM or AF). In the paramagnetic state, the insertion of iron gives rise to FM-like behavior as seen in $\chi(T)$ (T range 30–25 K, Fig. 11). In the AF state of the pure compound, the two nearest-neighbor Ni moments in adjacent layers orient antiparallel to one another and the interaction of the iron by symmetry cancels out, giving rise to frustration and to spin-glass-like behavior as observed (see Fig. 11). We feel that the doped system is an excellent candidate for the newly studied class of layered planar Ising models.[38]

Although long-range order associated with iron impurities was not observed, the strong influence that these impurities have on the nature of the transition implies some degree of regularity in their inclusion. Also, the results suggest that iron impurities between the planes, in the tunnels that the Li ions occupy, are localized in fixed positions. Thus, although charge compensation arguments suggest the creation of vacancies in the channels as iron replaces Li ions, the iron atoms in the channels would obstruct Li ionic free hopping. This picture is consistent with recent NMR studies[13,14] and with the observation that thermal motion of Li ions is suppressed (Tables I and III) as the system is doped.

ACKNOWLEDGMENTS

D.V. and J.L.Z. thank the Solid State Division at Oak Ridge National Laboratory for the technical support extended during the neutron scattering experiments. Ames Laboratory is operated for the U.S. Department of Energy by Iowa State University under Contract No. W-7405-Eng-82. The work at Ames was supported by the Director for Energy Research, Office of Basic Energy Sciences. ORNL is managed for the U.S. DOE by Lockheed Martin Energy Research Corporation under Contract No. DE-AC05-960R22464. G.E.B., P.P., and T.R. thank Fapesp and CNPq (Brazil) for financial help. Part of this work was done with the financial help of the Basque Government (Spain).

[1] T. Kanazawa, *Inorganic Phosphate Materials* (Elsevier, Tokyo, 1993).

[2] F. Hanic, M. Handlovič, K. Burdová, and J. Majling, J. Crystallogr. Spectroscopic Res. **12**, 99 (1982).

[3] H. D. Megaw, *Crystal Structures—A Working Approach* (Saunders, Philadephia, 1973), p. 249.

[4] *Ordering in Two Dimensions*, edited by S. K. Sinha (North-Holland, Amsterdam, 1980).

[5] I. S. Pronin, S. E. Sigaryov, and A. A. Vashman, Solid State Ionics **38**, 9 (1990).

[6] I. S. Pronin, A. A. Vashman, and S. E. Sigaryov, Phys. Rev. B **48**, 16 463 (1993).

[7] A. A. Vashman, I. S. Pronin, and S. E. Sigaryov, Solid State Ionics **58**, 201 (1992).

[8] R. P. Santoro, R. E. Newnham, and S. Nomura, J. Phys. Chem. Solids **27**, 655 (1966).

[9] R. P. Santoro, D. J. Segal, and R. E. Newnham, J. Phys. Chem. Solids **27**, 1192 (1966).

[10] R. P. Santoro and R. E. Newnham, Acta Crystallogr. **22**, 344 (1967).

[11] J. M. Mays, Phys. Rev. **131**, 38 (1963).

[12] Santoro and co-workers did not determine the full magnetic structure of $LiNiPO_4$ because of the low neutron scattering intensities of the magnetic Bragg reflections.

[13] A. Goñi, T. J. Bonagamba, M. A. Silva, H. Panepucci, T. Rojo, and G. E. Barberis, J. Appl. Phys. **84**, 416 (1998); A. Goñi, L. Lezama, G. E. Barberis, J. L. Pizarro, M. I. Arriortua, and T. Rojo, J. Magn. Magn. Mater. **164**, 251 (1996); A. Goñi, J. L. Pizarro, L. M. Lezama, G. E. Barberis, M. I. Arriortua, and T. Rojo, J. Mater. Chem. **6**, 412 (1996).

[14] A. Goñi, Ph.D. thesis, Facultad de Ciencias, Universidad del País Vasco, Spain, 1997.

[15] L. Fournes (private communication).

[16] A. C. Larson, R. B. Von Dreele, and M. Lujan, Jr., computer code GSAS, Generalized Structure Analysis System, Neutron Scattering Center, Los Alamos National Laboratory, 1990.

[17] S. Geller and J. L. Duran, Acta Crystallogr. **18**, 258 (1960).
[18] I. Abrahams and K. S. Easson, Acta Crystallogr., Sect. C: Cryst. Struct. Commun. **49**, 925 (1993).
[19] G. E. Bacon, *Neutron Diffraction*, 3rd. ed. (Oxford University Press, New York, 1975).
[20] The prominent lowest-order magnetic reflection (0 1 0) strongly rules out a model in which magnetic moment pointing in the *b* direction [Eq. (2)].
[21] L. Onsager, Phys. Rev. **65**, 117 (1944); C. N. Yang, *ibid.* **85**, 809 (1952). Onsager has shown that for $T \geqslant T_N$ the correlation length $\xi = [\ln \coth(J_{2D}/T) - 2J_{2D}/T]^{-1}$ with finite short-range order.
[22] L. P. Regnault and J. Rossat-Mignod, in *Magnetic Properties of Layered Transition Metal Compounds*, edited by L. J. de Jongh (Kluwer Academic, Dordrecht, 1990), p. 271.
[23] B. J. Birgeneau, J. Als-Nielsen, and G. Shirane, Phys. Rev. B **16**, 280 (1977).
[24] L. J. de Jongh, in *Magnetic Properties of Layered Transition Metal Compounds*, edited by L. J. de Jongh (Kluwer Academic, Dordrecht, 1990), p. 1.
[25] A. Abragam and B. Bleaney, *Electron Paramagnetic Resonance of Transition Metals* (Clarendon Press, Oxford, 1970), pp. 363–471.
[26] C. J. Ballhausen, *Introduction to Ligand Field Theory* (McGraw-Hill, New York, 1962), pp. 137–139, and 261–273; *Molecular Electronic Structures of Transition Metal Complexes* (McGraw-Hill, New York, 1979), pp. 73–84.
[27] K. D. Bowers and J. Owen, Rep. Prog. Phys. **18**, 304 (1955).
[28] W. M. Walsh, Jr. and N. Bloembergen, Phys. Rev. **75**, 904 (1957).
[29] M. Plischke and B. Bergersen, *Equilibrium Statistical Physics* (Prentice-Hall, Englewood Cliffs, NJ, 1989).
[30] M. E. Fisher, Rep. Prog. Phys. **30**, 615 (1967).
[31] M. F. Sykes and M. E. Fisher, Physica (Amsterdam) **28**, 919 (1962).
[32] M. E. Fisher, J. Math. Phys. **4**, 125 (1963).
[33] J. L. Zarestky, D. Vaknin, G. Barberis, and T. Rojo (unpublished).
[34] D. J. Breed, K. Gilijamse, and A. R. Miedema, Physica (Amsterdam) **45**, 205 (1969).
[35] E. J. Samuelson, Phys. Rev. Lett. **31**, 936 (1973).
[36] H. Ikeda and K. Hirakawa, Solid State Commun. **14**, 529 (1974).
[37] G. S. Pawley, R. H. Swendsen, D. J. Wallace, and G. Wilson, Phys. Rev. B **29**, 4030 (1984).
[38] L. V. Mikheev and M. E. Fisher, Phys. Rev. B **49**, 378 (1994).